Journal of Hazardous Materials 166 (2009) 939–944

Contents lists available at ScienceDirect

Journal of Hazardous Materials

journal homepage: www.elsevier.com/locate/jhazmat

Research article

Enhanced photocatalytic activity of S-doped TiO_2–ZrO_2 nanoparticles under visible-light irradiation

Guohui Tian, Kai Pan, Honggang Fu*, Liqiang Jing, Wei Zhou

Key Laboratory of Functional Inorganic Material Chemistry (Heilongjiang University), Ministry of Education, Laboratory of Physical Chemistry, School of Chemistry and Materials Science, Heilongjiang University, Harbin, Heilongjiang 150080, China

ARTICLE INFO

Article history:
Received 1 September 2008
Received in revised form
26 November 2008
Accepted 26 November 2008
Available online 3 December 2008

Keywords:
S-doped TiO_2
Visible-light absorption
Photocatalysis
Hydroxyl radical

ABSTRACT

Porous nanocrystalline S-doped TiO_2–ZrO_2 visible-light photocatalysts were prepared through a one-step method. The resulting materials were characterized by X-ray diffraction (XRD), N_2 adsorption–desorption measurements, transmission electron microscopy (TEM), X-ray photoelectron spectroscopy (XPS), UV–vis diffuse reflectance spectra (DRS), Fourier transform infrared spectra (FT-IR) and electron paramagnetic resonance (ESR). It was found that modification by ZrO_2 could effectively inhibit phase transformation, enhance visible-light absorption, and possess more surface hydroxyl groups. The photocatalytic activity of S-doped TiO_2–ZrO_2 was higher than that of unmodified S-doped TiO_2 and Degussa P25. The enhanced photocatalytic activity could be attributed to the higher specific area, smaller crystal size, porous structure and more surface hydroxyl groups in the catalyst.

1. Introduction

TiO_2 has been widely used as an efficient photocatalyst for the photogradation of organic pollutants in water owing to its inexpensiveness, strong oxidizing power, non-toxicity and long-term photostability [1–4]. However, it can be activated only under UV light irradiation because of its large energy band gap (3.2 eV for anatase TiO_2) [5,6]. For further improvement of effective utilization of the solar energy, considerable efforts have been made to shift its photocatalytic activity to the visible-light region. One of earlier approaches was the doping of TiO_2 with transition-metal elements [7–9]. However, the disadvantage of cationic dopants is that they often show a weak absorption in the visible-light region [10]. For further improvement of effective utilization of solar energy, nonmetal doping (N, S, B, C) has been carried out to prepare visible sensitive photocatalyst via band gap narrowing of photocatalyst [11–21]. Among which, S dopant is often incorporated as anion, cation or both anion and cation to take the place of Ti ion or/and oxygen in the lattice of TiO_2, and the S-doped TiO_2 powders show high photocatalytic activity under visible-light [21–23]. In general, the preparation of S-doped TiO_2 powder mainly includes wet chemical methods such as co-precipitation, sol gel, and hydrothermal [24–26]. These methods are usually performed under relatively low temperature conditions because the prepared S-doped TiO_2 materials usually have a low thermal stability. Otherwise, the doped nonmetal element will be replaced by oxygen again under high thermal treatment. However, low temperature condition usually leads to the existence of other undesired impurified materials, low crystallinity and lots of surface defects, which are not helpful to the improvement of photocatalytic activity.

The introduction of a second metal oxide (La_2O_3, SiO_2, ZrO_2, etc.) was proved to be an effective route to improve the thermal stability and UV light photocatalytic activity of TiO_2 [27–29]. Among them, a mixed system with ZrO_2 and TiO_2 was widely investigated in the photocatalysis field by our and other groups [29,30], the addition of ZrO_2 in TiO_2 could not only enhance the phase stability for the phase transformation of pure TiO_2 and N-doped TiO_2 particles from anatase-to-rutile but also stabilize the surface area and nitrogen incorporated in the catalyst, and thus enhanced photocatalytic activity.

In the present research, mesoporous S-doped TiO_2–ZrO_2 visible-light photocatalysts were successfully prepared on the basis of our previous study [30]. The introduction of ZrO_2 in the catalyst could significantly enhance the thermal stability of the S-doped TiO_2 and extend the absorption to visible-light region. The photocatalytic activity of the S-doped TiO_2–ZrO_2 photocatalysts has been investigated in the visible-light region for the decomposition of rhodamine B (RB) as a model pollutant. A considerably enhanced photocatalytic activity was found for the S-doped TiO_2–ZrO_2

* Corresponding author. Tel.: +86 451 86608458; fax: +86 451 86673647.
E-mail address: fuhg@vip.sina.com (H. Fu).

0304-3894/$ – see front matter © 2008 Elsevier B.V. All rights reserved.
doi:10.1016/j.jhazmat.2008.11.090

in comparison to the S-doped TiO_2 and commercial Degussa P25.

2. Experimental

2.1. Preparation of catalysts

Tetrabutyl titanate and $ZrOCl_2{\cdot}8H_2O$ were used as the inorganic sources, amphiphilic triblock copolymer Pluronic P123 (PEO_{20}–PPO_{70}–PEO_{20}, MW = 5800, Aldrich, PEO = poly (ethyleneglycol), PPO = poly (propylene glycol)) and thiourea were used as the surfactant and sulfur source, respectively. 4 g HCl (10 mol l^{-1}) was slowly added to 6.8 g tetrabutyl titanate under vigorous stirring at room temperature. After 20 min, a mixture solution of 0.39 g thiourea and 2.0 g P123 dissolved in ethanol was added, after magnetic stirring for 2 h, 0.52 g $ZrOCl_2{\cdot}8H_2O$ was added into the mixture at a Zr/(Zr + Ti) molar ratio of 0.075 and vigorously stirred for 6 h. After aging at room temperature for 24 h, the obtained sol solution was dried at 40 °C for 5 h until a dry gel was gotten. This gel was milled and calcined in air for 4 h at 400, 500 and 600 °C, respectively, with a constant heating rate of 1 °C min^{-1}. A sample without any $ZrOCl_2{\cdot}8H_2O$ was also prepared to compare the results.

2.2. Characterization

X-ray diffraction patterns were carried out on a Rigaku D/MAX X-ray diffractometer, using Cu Ka radiation with λ = 0.15406 nm. The accelerating voltage and applied current were 20 kV and 20 mA, respectively. After samples had been vacuum-dried at 200 °C overnight, nitrogen adsorption–desorption isotherms were collected on an AUTOSORB-1 (Quantachrome Instruments) nitrogen adsorption apparatus at 77 K. The pore size distribution plots were obtained by the Barret–Joyner–Halenda (BJH) model. Transmission electron microscopy (TEM) and high-resolution TEM (HRTEM) images of samples were recorded in a JEOL 2010 microscope with a 200 kV accelerating voltage. X-ray photoelectron spectroscopy (XPS) measurements were performed with Thermo ESCALAB 250. Bulk sulfur concentrations of the samples were determined by Thermo ICAP6300 inductively coupled plasma-atomic emission spectrometry (ICP-AES). Before test, the sample powders were firstly digested using a mixture solution of HF and HNO_3 on a sand bath at 150–200 °C until complete dissolution. UV–vis diffuse reflectance spectra (DRS) were determined by a UV–vis spectrophotometer (Shimadzu UV-2550). Fourier transform infrared spectra (FT-IR) were recorded in a PerkinElmer spectrum one system. The samples were mixed with KBr and the concentrations of the samples were kept round 0.25–0.3%. The mixture was pressed under 10 tons cm^{-2} to get a 300 mg pellet. Electron paramagnetic resonance (ESR) experiment was conducted for the determination of $^{\bullet}OH$ generated using 5, 5-dimethyl-1-pyrolin-N-oxide (DMPO) as a nitron spin-trapping reagent, the ESR spectrum was measured at room temperature with an ESR spectrometer (Bruker EMX-8/2.7 ESR spectrometer).

2.3. Measurement of photocatalytic activity

The photodegradation experiments were performed in a slurry reactor containing 80 ml of a 10 mg l^{-1} solution of rhodamine B (RB) and 0.1 g of catalyst. A 380 W Xe lamp was used as a visible-light source, and a 410 nm cutoff filter was placed above the reactor to cutoff UV light, the average light intensity was 50 mW cm^{-2}. Prior to irradiation, the suspension was kept in the dark under stirring for 30 min to ensure the establishing of an adsorption/desorption equilibrium. At given time intervals, 2 ml aliquots were collected from the suspension and immediately centrifuged, the concentration of RB after illumination was determined at 554 nm using a UV–vis spectrophotometer (Shimadzu UV-2550).

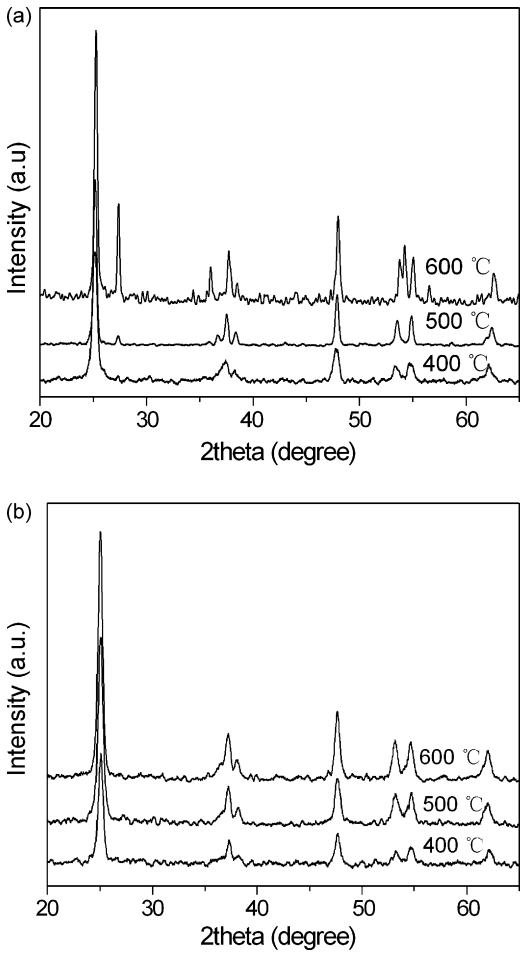

Fig. 1. XRD patterns of (a) S-TiO_2 and (b) S-TiO_2–ZrO_2 samples after calcination at 400, 500 and 600 °C.

3. Results and discussion

3.1. XRD analysis

Fig. 1a and b shows the XRD patterns of the S-TiO_2 and S-TiO_2–ZrO_2 samples calcined at different temperatures, respectively. The average crystallite sizes of the catalysts are calculated using the Scherrer equation and the values are listed in Table 1. At 400 °C, the two samples display pure anatase phase, the crystal sizes are 10.6 and 6.9 nm for S-TiO_2 and S-TiO_2–ZrO_2, respectively. For the S-TiO_2 sample, the anatase-to-rutile phase transformation occurs at 500 °C. However, the S-TiO_2–ZrO_2 sample shows 100% anatase phase even at 600 °C, and the crystal size of anatase in the S-TiO_2–ZrO_2 sample still maintains 11.6 nm. Meanwhile, no tetragonal ZrO_2 phase can be seen at 400, 500 and 600 °C. Our previous study shows that tetragonal ZrO_2 phase can only be observed at or above 800 °C [30]. Therefore, it can be thought that the mixed oxide materials are TiO_2–ZrO_2 solid solution composites. The results indicate that the introduction of ZrO_2 can effectively suppress the anatase-to-rutile phase transformation and crystal growth of S-doped TiO_2 particles during the calcination process, which is consistent with the previous results reported above [29,30].

Table 1
Physicochemical properties of two series of S-TiO_2 and S-TiO_2–ZrO_2 samples calcined at 400, 500 and 600 °C.

Sample	Calcination temperature (°C)	Anatase (wt%)[a]	Rutile (wt%)[a]	Crystal size (nm)[a]	S_{BET} ($m^2\ g^{-1-}$)[b]	Pore size (nm)[b]
S-TiO_2	400	100	0	10.6 (A)	114	3.2
	500	95	5	21.5 (A), 29.8 (R)	23	9.8
	600	62	38	31.5 (A), 41.2 (R)	2	–
S-TiO_2–ZrO_2	400	100	0	6.9 (A)	175	3.5
	500	100	0	8.5 (A)	116	3.8
	600	100	0	11.6 (A)	25	–

[a] Phase content and crystal size measured from XRD, A and R denote anatase and rutile, respectively.
[b] S_{BET}, BET surface area; mean pore size measured from N_2 adsorption isotherm branch.

3.2. BET surface areas and pore structure analysis

In order to investigate the surface area and pore structure of the catalysts, nitrogen adsorption–desorption measurement was carried out. The data parameters are summarized in Table 1. Nitrogen adsorption–desorption isotherms (inseted) and their BJH pore size distributions of the S-TiO_2 and S-TiO_2–ZrO_2 samples calcined at 500 °C are shown in Fig. 2. The insets in Fig. 2b exhibits a type IV isotherm with an inflection of nitrogen adsorbed volume at $P/P_0 = 0.45$ (type H2 hysteresis loop), being representative of mesoporosity in the S-TiO_2–ZrO_2 sample. The pore size distributions in Fig. 2a and b show that the S-TiO_2–ZrO_2 sample has a very narrow pore size distribution with an average pore diameter at ca. 3.8 nm. However, the S-TiO_2 sample has a wide pore size distribution and big pores with average pore size of 9.8 nm resulted from the big crystallites aggregation. The specific surface area of S-TiO_2–ZrO_2 sample calcined at 500 °C is 116 $m^2\ g^{-1}$, and it remained as large as 25 $m^2\ g^{-1}$ even after calcination at 600 °C. However, the specific surface area of S-TiO_2 sample calcined at 500 and 600 °C is only 23 and 2 $m^2\ g^{-1}$, respectively. This should be due to crystallite growth and collapse of the porous framework. The relatively high surface area of S-TiO_2–ZrO_2 samples confirms that the introduction of ZrO_2 can significantly stabilize the porous structure and reinforce the thermal stability of S-TiO_2–ZrO_2.

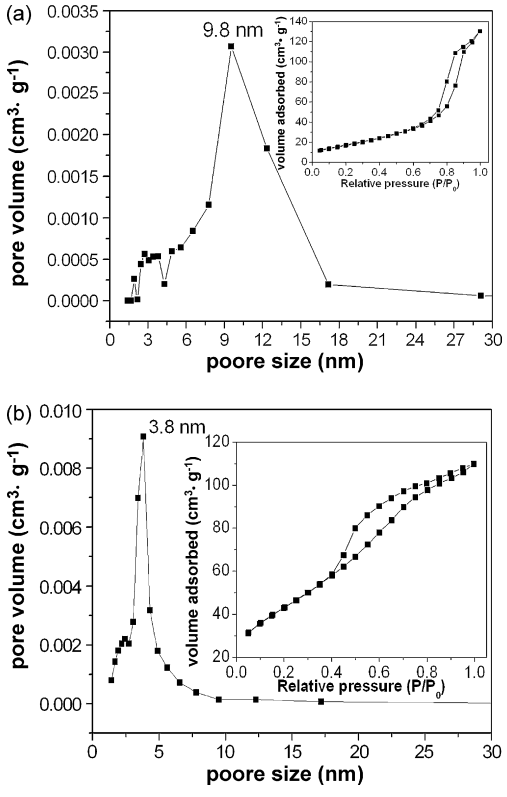

Fig. 2. Pore size distributions of the S-TiO_2 (a) and S-TiO_2–ZrO_2 (b) samples after calcination at 500 °C. Inset: N_2 adsorption–desorption isotherm.

3.3. TEM analysis

Fig. 3 shows the TEM images of the prepared S-TiO_2 and S-TiO_2–ZrO_2 samples calcined at 500 °C. Compared with the control (Fig. 3a and b), for the S-TiO_2 sample calcined at 500 °C, no porous structure is found, and the particles (20–30 nm) are more larger than those (6–10 nm) of the S-TiO_2–ZrO_2 sample calcined at 500 °C. Fig. 3c presents the high magnification image of Fig. 3b, some disordered porous structure (locations marked with black circles) and many randomly oriented nanocrystallites with sets of clearly resolved lattice fringes were observed. The results indicate that the introduction of ZrO_2 can effectively inhibit the excessive crystal growth and stabilize the porous structure, which is consistent with XRD and N_2-sorption measurements.

3.4. XPS analysis

Fig. 4 shows the S 2p XPS spectra of S-TiO_2 and S-TiO_2–ZrO_2 samples calcined at 500 °C. In both samples, a peak at 168.5 eV could be observed and assigned to S^{6+} [31]. The peak intensity of S-TiO_2–ZrO_2 sample is much stronger than that of S-TiO_2 sample, indicating that the surface sulfur content (1.10%) in S-TiO_2/ZrO_2 sample is larger than that (0.65%) in S-TiO_2 sample. Additionally, the bulk S concentrations of the S-TiO_2 and S-TiO_2–ZrO_2 samples calcined at 500 °C are also determined by ICP-AES method, bulk sulfur concentrations are 0.45 and 0.79%, respectively. Apparently, the introduction of ZrO_2 can effectively stabilize the sulfur in the TiO_2 matrix. Moreover, for the same sample, the surface sulfur concentration is larger than that of bulk sulfur concentration. The differences between XPS and ICP-AES results might be due to surface accumulation of sulfur.

3.5. UV–vis diffuse reflectance spectra analysis

The UV–vis diffuse reflectance spectra of the S-TiO_2 and S-TiO_2–ZrO_2 samples calcined at different temperatures are shown in Fig. 5a and b, respectively. It can be seen that, compared to the spectrum of pure TiO_2, the absorption spectra of S-TiO_2 and S-TiO_2–ZrO_2 samples show obvious visible-light absorption. However, with the increase of calcination temperature, the decrease in absorption for S-TiO_2 sample is larger than that for the corresponding S-TiO_2–ZrO_2 sample, which might be due to structural or superficial changes and the gradual decrease of sulfur content. Moreover, at the same calcination temperature, S-TiO_2–ZrO_2 has a larger red shift of absorption band edge than S-TiO_2. Therefore, the introduction of ZrO_2 can effectively enhance visible-light absorption.

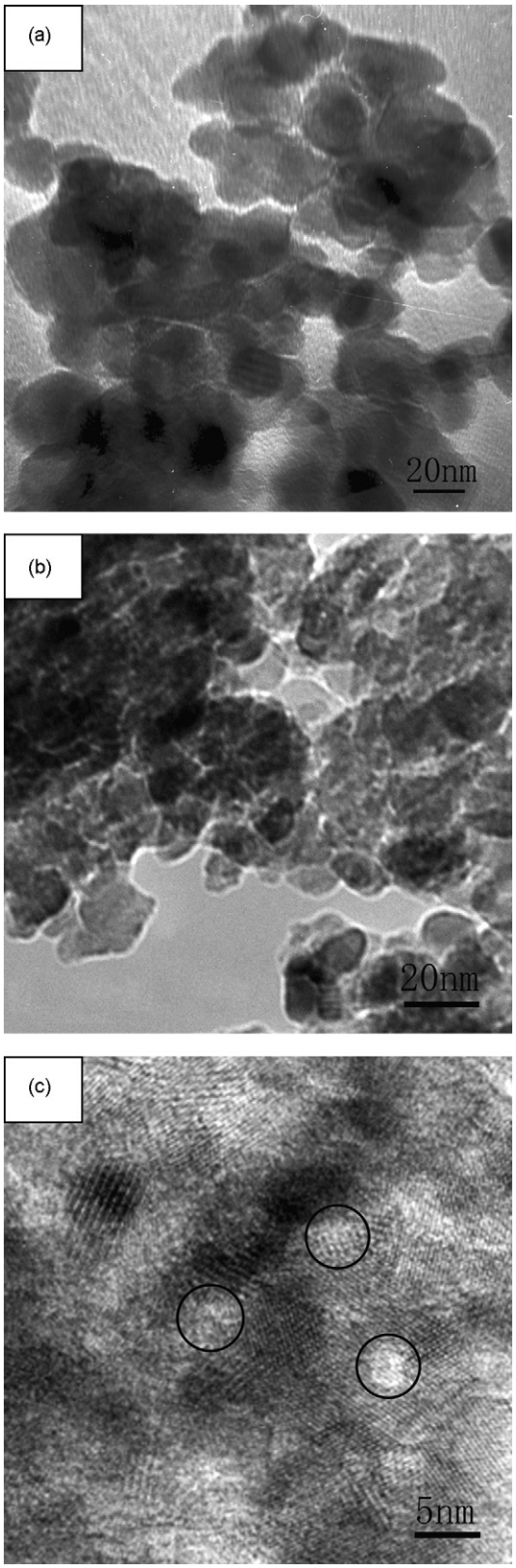

Fig. 3. TEM images of S-TiO_2 (a), and S-TiO_2–ZrO_2 (b and c) samples after calcination at 500 °C.

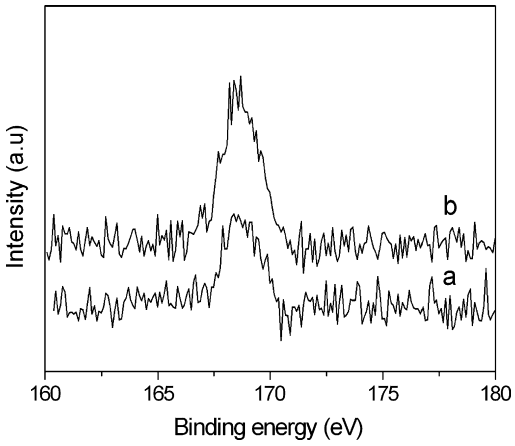

Fig. 4. XPS spectra of S 2p region of S-TiO_2 (a) and S-TiO_2–ZrO_2 (b) samples after calcination at 500 °C.

3.6. FT-IR spectra analysis

The FT-IR spectra of S-TiO_2 and S-TiO_2–ZrO_2 samples calcined at 500 °C are shown in Fig. 6. Several peaks at 1250–900 cm^{-1} were observed on the spectra for both samples. The peaks at 1218, 1150, 1040, and 975 cm^{-1} can be attributed to the characteristic frequencies of a bidentate SO_4^{2-} co-ordinated to metal Ti^{4+} [32]. Such an interaction between SO_4^{2-} and Ti^{4+} is thought to be a driving force in the generation of a large amount of surface acidic sites on solid acids of sulfated metal oxides [32,33]. Two peaks at 3402 and 1640 cm^{-1} are assigned to the surface adsorbed water and hydroxyl groups [34]. Obviously, compared with that in S-TiO_2, the intensity

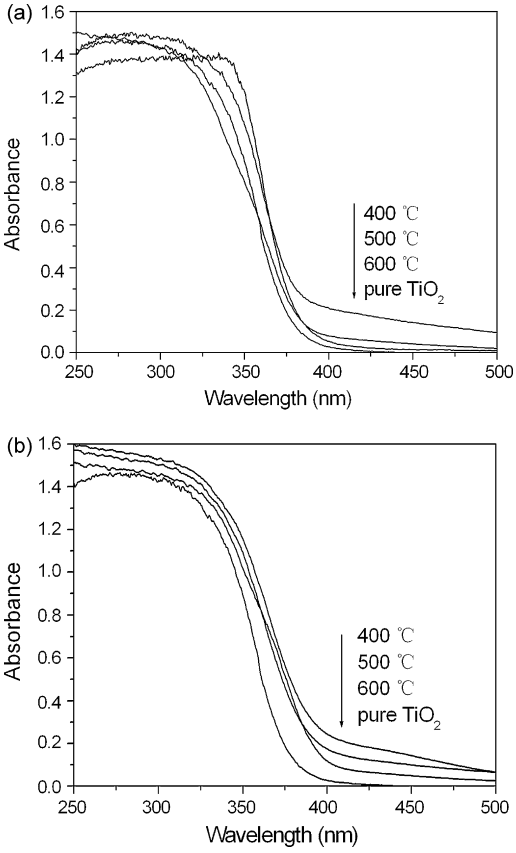

Fig. 5. UV–vis diffuse reflectance spectra of (a) S-TiO_2 and (b) S-TiO_2–ZrO_2 samples after calcination at 400, 500 and 600 °C.

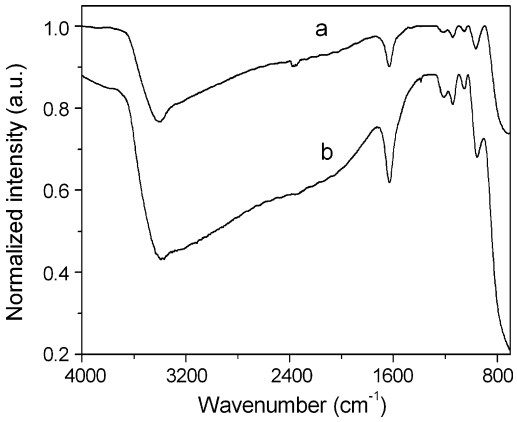

Fig. 6. FT-IR spectra of S-TiO_2 (a) and S-TiO_2–ZrO_2 (b) samples after calcination at 500 °C.

of the two peaks in S-TiO_2–ZrO_2 is much stronger. This indicates that the introduction of ZrO_2 makes the catalyst possess more surface hydroxyl groups, which favors not only the trapping of electrons to enhance the separation efficiency of electron-hole pair but also the forming of surface free radical (•OH) to enhance the photocatalytic degradation of RB [34,35].

3.7. ESR analysis

We employed the ESR spin-trap technique (with DMPO) to probe the nature of the reactive oxygen species generated on the surface of catalysts under visible-light irradiation. Fig. 7 shows the typical ESR spectrum of the DMPO–•OH spin adduct. The characteristic quartet peaks of the DMPO–•OH adduct with a 1:2:2:1 intensity were obviously observed in the suspension of S-TiO_2 and S-TiO_2–ZrO_2 samples calcined at 500 °C, which is consistent with the similar spectra reported by others for the DMPO–•OH adduct [36]. The phenomenon of the experiment indicates the formation of hydroxyl radicals from the S-doped samples under visible irradiation. Moreover, the peak intensity of DMPO–•OH adduct generated by S-TiO_2 sample was less than that of S-TiO_2–ZrO_2 sample, indicating a larger production of •OH for S-TiO_2–ZrO_2 sample, which is consistent with the FT-IR test results because of fact that hydroxyl radical originates from the oxidation of surface chemisorbed water and hydroxyl groups.

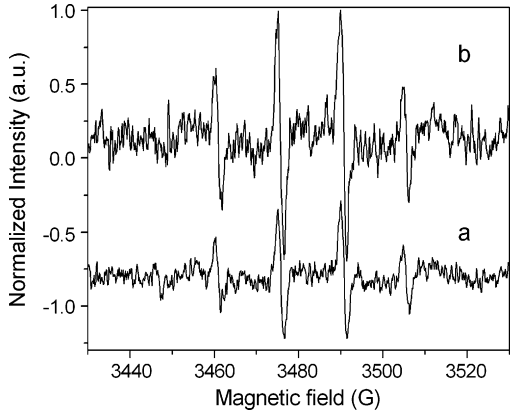

Fig. 7. Comparison of the intensity of DMPO–•OH adduct signal in (a) S-TiO_2 and (b) S-TiO_2–ZrO_2 dispersion (the signals were recorded after visible-light illumination for 100 s, initial DMPO concentration: 9.6 g l^{-1}).

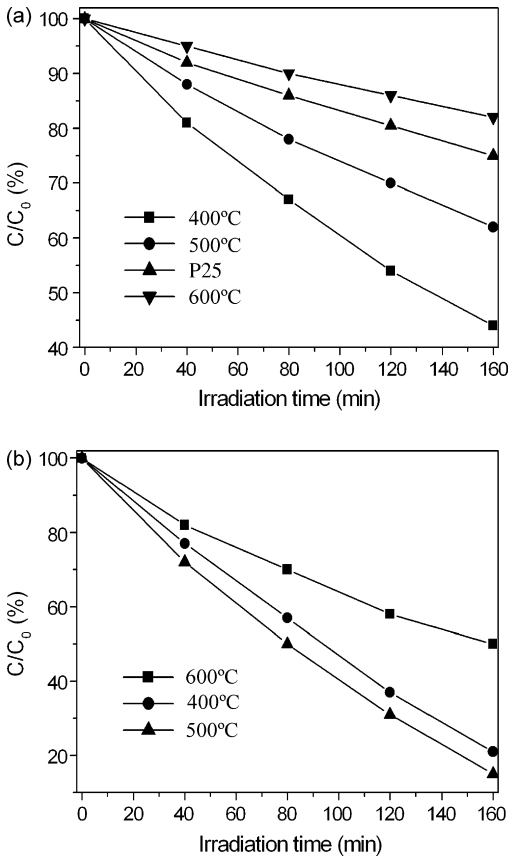

Fig. 8. Visible-light-induced catalytic degradation of RB in presence of (a) S-TiO_2, Degussa P25 and (b) S-TiO_2–ZrO_2 catalysts after calcination at 400, 500 and 600 °C.

3.8. Photocatalytic activity

To evaluate and compare the photocatalytic activity of the S-TiO_2 and S-TiO_2–ZrO_2 samples calcined at different temperatures, the reactions of RB degradation were performed as photoreaction probes under visible-light irradiation, respectively. The photocatalytic behavior of Degussa P25 was also measured as a reference. Results of the photocatalytic evaluation are shown in Fig. 8a and b. As expected, the S-doped TiO_2 is active under visible-light, while the photocatalytic activity of S-TiO_2 is limited, and decreases gradually with increasing calcination temperature because of the larger particle size, smaller specific surface area and the limited utilization of visible-light. At the calcination temperature of 400 °C, the degradation rate of RB is 56%, but it drops to 18% at 600 °C. However, when S-doped TiO_2 was modified by ZrO_2, the photocatalytic activity was further enhanced, and the photocatalytic activity increased gradually with the increase of calcination temperature, and then decreased. As is shown in Fig. 8, the S-TiO_2–ZrO_2 sample calcined at 500 °C shows the maximum activity among all the samples, the degradation rate of RB is 85% within 160 min, which could be attributed to its comparatively high surface area, small crystalline size, porous structure, well-crystalline anatase phase and intense absorption in the visible-light region. The decrease in the photocatalytic activity of S-TiO_2–ZrO_2 calcined at 600 °C is due to its small surface area, large crystallite size and relative low visible-light absorption. On the other hand, only 25% RB was degraded on commercial Degussa P25.

It has been proved in our previous paper that the modification of ZrO_2 can increase the photocatalytic activity of TiO_2 under UV light illumination due to its large surface area, small crystalline size and good crystallinity [30]. These are also the reasons that

S-TiO_2–ZrO_2 sample has higher activity than the corresponding S-TiO_2 sample. The large surface area can provide more surface sites for the adsorption of reactants molecules such as surface chemisorbed water and hydroxyl group, which are favorable for the formation of hydroxyl radicals with high oxidation capability, just these hydroxyl radicals can oxidize adsorbed various organic molecules. ESR measurement results above confirm the content of hydroxyl radicals generated from the S-TiO_2–ZrO_2 sample is larger than that of hydroxyl radicals generated from the S-TiO_2 sample under visible-light irradiation, apparently, this is in agreement with photocatalytic test. Furthermore, the introduction of ZrO_2 enhance the absorption of S-TiO_2–ZrO_2 in the visible-light region compared with the corresponding S-TiO_2, the intense absorption in the UV–vis light region indicated that more photo-generated electrons and holes can participate in the photocatalytic reactions. Additionally, the existence of more surface acidic sites might also favor the photodecomposition of organics, and such further improve the photocatalytic performance [32].

4. Conclusions

In summary, ZrO_2 modified S-doped TiO_2 visible-light photocatalysts were successfully prepared by a simple method. The introduction of ZrO_2 could effectively suppress phase transformation of anatase-to-rutile and stabilize the sulfur in the S-TiO_2–ZrO_2 matrix, and thus enhancing visible-light absorption compared with the corresponding non-modified S-TiO_2 sample. The visible-light photocatalytic activities of S-TiO_2–ZrO_2 samples were higher than that of S-TiO_2 samples and commercial Degussa P25. The high photocatalytic activities of the as-prepared S-TiO_2–ZrO_2 can be attributed to the synergetic effects of large specific area, high crystallinity, intense absorption in the visible-light region, more surface hydroxyl groups and surface acidic sites in the catalyst.

Acknowledgments

The work was supported by the Key Program Projects of National Natural Science Foundation of China (No. 20431030), the National Natural Science Foundation of China (Nos. 20671032 and 20676027), the Program for New Century Excellent Talents in University (NCET-07-0259), the Key Program Projects of the Province Natural Science Foundation of Heilongjiang Province (No. ZJG0602-01).

References

[1] X.b. Chen, S.S. Mao, Titanium dioxide nanomaterials: synthesis, properties, modifications, and applications, Chem. Rev. 107 (2007) 2891–2959.
[2] P.G. Li, J.N. Khor, A. Brucato, Modeling of an annular photocatalytic reactor for water purification: oxidation of pesticides, Environ. Sci. Technol. 38 (2004) 3737–3745.
[3] P.V. Kamat, R. Huehn, R.A. Nicolaescu, "Sense and Shoot" approach for photocatalytic degradation of organic contaminants in water, J. Phys. Chem. B 106 (2002) 788–794.
[4] M.I. Litter, Heterogeneous photocatalysis: transition metal ions in photocatalytic systems, Appl. Catal. B: Environ. 23 (1999) 89–114.
[5] K.E. Karakitsou, X.E. Verykios, Effects of altervalent cation doping of titania on its performance as a photocatalyst for water cleavage, J. Phys. Chem. 97 (1993) 1184–1189.
[6] Y. Aita, M. Komatsu, S. Yin, T. Sato, Phase-compositional control and visible light photocatalytic activity of nitrogen-doped titania via solvothermal process, J. Solid State Chem. 177 (2004) 3235–3238.
[7] M. Anpo, M. Takeuchi, The design and development of highly reactive titanium oxide photocatalysts operating under visible light irradiation, J. Catal. 216 (2003) 505–516.
[8] S. Klosek, D. Raftery, Visible light driven V-doped TiO_2 photocatalyst and its photooxidation of ethanol, J. Phys. Chem. B 105 (2001) 2815–2819.
[9] H. Haick, Y. Paz, Long-range effects of noble metals on the photocatalytic properties of titanium dioxide, J. Phys. Chem. B 107 (2003) 2319–2326.
[10] S.X. Liu, Z.P. Qu, X.W. Han, Effect of silver modification on the photocatalytic activity of TiO_2 photocatalysis, Chin. J. Catal. 25 (2004) 133–138.
[11] R. Asashi, T. Morikawa, T. Ohwaki, K. Aoki, Y. Taga, Visible-light photocatalysis in nitrogen doped titanium oxides, Science 293 (2001) 269–271.
[12] S.U.M. Khan, M. Al-shahry, W.B. Ingler Jr., Efficient photochemical water splitting by a chemically modified N-TiO_2, Science 297 (2002) 2243–2244.
[13] W. Su, Y. Zhang, Z. Li, L. Wu, X. Wang, J. Li, X.Z. Fu, Multivalency iodine doped TiO_2: preparation, characterization, theoretical studies, and visible-light photocatalysis, Langmuir 24 (2008) 3422–3428.
[14] W.J. Ren, Z.H. Ai, F.L. Jia, L.Z. Zhang, X.X. Fan, Z.G. Zou, Low temperature preparation and visible light photocatalytic activity of mesoporous carbon-doped crystalline TiO_2, Appl. Catal. B: Environ. 69 (2007) 138–144.
[15] G. Shen, J.H. Cho, J.K. Yoo, G.-C. Yi, C.J. Lee, Synthesis and optical properties of S-doped ZnO nanostructures: nanonails and nanowires, J. Phys. Chem. B 109 (2005) 5491–5496.
[16] X. Chen, C. Burda, The electronic origin of the visible-light absorption properties of C-, N- and S-doped TiO_2 nanomaterials, J. Am. Chem. Soc. 130 (2008) 5018–5019.
[17] H. Li, X. Zhang, Y. Huo, J. Zhu, Supercritical preparation of a highly active S-doped TiO_2 photocatalyst for methylene blue mineralization, Environ. Sci. Technol. 41 (2007) 4410–4414.
[18] S. In, A. Orlov, R. Berg, F. Garcia, S. Pedrosa-Jimenez, M.S. Tikhov, D.S. Wright, R.M. Lambert, Effective visible light-activated B-doped and B, N-codoped TiO_2 photocatalysts, J. Am. Chem. Soc. 129 (2007) 13790–13791.
[19] N. Lu, X. Quan, J. Li, S. Chen, H. Yu, G. Chen, Fabrication of boron-doped TiO_2 nanotube array electrode and investigation of its photoelectrochemical capability, J. Phys. Chem. C 111 (2007) 11836–11842.
[20] L. Lin, R.Y. Zheng, J.L. Xie, Y.X. Zhu, Y.C. Xie, Synthesis and characterization of nitrogen co-doped titania, Appl. Catal. B: Environ. 76 (2007) 196–202.
[21] T. Ohno, T. Mitsui, M. Matsumura, Photocatalytic activity of S-doped TiO_2 photocatalyst under visible light, Chem. Lett. 32 (2003) 364–365.
[22] T. Umebayashi, T. Yamaki, H. Ito, K. Asai, Band gap narrowing of titanium dioxide by sulfur doping, Appl. Phys. Lett. 81 (2002) 454–456.
[23] J.G. Yu, M.H. Zhou, B. Cheng, X.J. Zhao, Preparation, characterization and photocatalytic activity of in situ N, S-doped TiO_2 powders, J. Mol. Catal. A 246 (2006) 176–184.
[24] G.K. Zhang, X.M. Ding, F.S. He, X.Y. Yu, Preparation and photocatalytic properties of TiO_2 montmorillonite doped with nitrogen and sulfur, J. Phys. Chem. Solids 69 (2008) 1102–1106.
[25] W.K. Ho, J.C. Yu, S.C. Lee, Low-temperature hydrothermal synthesis of S-doped TiO_2 with visible light photocatalytic activity, J. Solid State Chem. 179 (2006) 1171–1176.
[26] S.X. Liu, X.Y. Chen, Visible light response TiO_2 photocatalyst realized by cationic S-doping and its application for phenol degradation, J. Hazard. Mater. 152 (2008) 48–55.
[27] B.M. Reddy, P.M. Sreekanth, E.P. Reddy, Y. Yamada, Q. Xu, H. Sakurai, T. Kobayashi, Surface characterization of La_2O_3–TiO_2 and V_2O_5/La_2O_3–TiO_2 catalysts, J. Phys. Chem. B 106 (2002) 5695–5700.
[28] S. Hong, M.S. Lee, S.S. Park, G. Lee, Synthesis of nanosized TiO_2/SiO_2 particles in the microemulsion and their photocatalytic activity on the decomposition of *p*-nitrophenol, Catal. Today 87 (2003) 99–105.
[29] X.C. Wang, J.C. Yu, Y.L. Chen, L. Wu, X.Z. Fu, ZrO_2-modified mesoporous nanocrystalline $TiO_{2-x}N_x$ as efficient visible light photocatalysts, Environ. Sci. Technol. 40 (2006) 2369–2374.
[30] W. Zhou, K.S. Liu, H.G. Fu, K. Pan, Multi-modal mesoporous TiO_2–ZrO_2 composites with high photocatalytic activity and hydrophilicity, Nanotechnology (2008), doi:10.1088/0957-4484/19/03/035610.
[31] P. Periyat, S.C. Pillai, D.E. McCormack, J. Colreavy, S.J. Hinder, Improved high-temperature stability and sun-light-driven photocatalytic activity of sulfur-doped anatase TiO_2, J. Phys. Chem. C 112 (2008) 7644–7652.
[32] X.C. Wang, J.C. Yu, P. Ping, X.X. Wang, W.Y. Su, X.Z. Fu, Probing of photocatalytic surface sites on SO_4^{2-}/TiO_2 solid acids by in situ FT-IR spectroscopy and pyridine adsorption, J. Photochem. Photobiol. A: Chem. 179 (2006) 339–347.
[33] J.R. Sohn, H.J. Kim, High catalytic activity of NiO-TiO_2/SO_4^{2-} for ethylene dimerization, J. Catal. 101 (1986) 428–433.
[34] G.H. Tian, H.G. Fu, L.Q. Jing, K. Pan, Synthesis and photocatalytic activity of stable nanocrystalline TiO_2 with high crystallinity and large surface area, J. Hazard. Mater. 161 (2009) 1122–1130.
[35] Y.D. Hou, X.C. Wang, L. Wu, X.F. Chen, Z.X. Ding, X.X. Wang, X.Z. Fu, N-Doped SiO_2/TiO_2 mesoporous nanoparticles with enhanced photocatalytic activity under visible-light irradiation, Chemosphere 72 (2008) 414–421.
[36] J.C. Yu, W.K. Ho, J.G. Yu, H.Y. Yip, P.K. Wong, J.C. Zhao, Efficient visible-light-induced photocatalytic disinfection on sulfur-doped nanocrystalline titania, Environ. Sci. Technol. 39 (2005) 1175–1179.